

Testing the space-time geometry around black hole candidates with the analysis of the broad $K\alpha$ iron line

Cosimo Bambi*

*Center for Field Theory and Particle Physics & Department of Physics,
Fudan University, 200433 Shanghai, China and
Arnold Sommerfeld Center for Theoretical Physics,
Ludwig-Maximilians-Universität München, D-80333 Munich, Germany*

(Dated: August 16, 2018)

Astrophysical black hole candidates are thought to be the Kerr black holes predicted by General Relativity, but there is not yet clear evidence that the geometry of the space-time around these objects is really described by the Kerr metric. In order to confirm the Kerr black hole hypothesis, we have to observe strong gravity features and check that they are in agreement with the ones predicted by General Relativity. In this paper, I study the broad $K\alpha$ iron line, which is often seen in the X-ray spectrum of both stellar-mass and super-massive black hole candidates and whose shape is supposed to be strongly affected by the space-time geometry. As found in previous studies in the literature, there is a strong correlation between the spin parameter and the deformation parameter; that is, the line emitted around a Kerr black hole with a certain spin can be very similar to the one coming from the space-time around a non-Kerr object with a quite different spin. Despite that, the analysis of the broad $K\alpha$ iron line is potentially more powerful than the continuum-fitting method, as it can put an interesting bound on possible deviations from the Kerr geometry independently of the value of the spin parameter and without additional measurements.

PACS numbers: 97.60.Lf, 98.62.Js, 04.50.Kd, 04.80.Cc

I. INTRODUCTION

Today we think the final product of the gravitational collapse is a black hole (BH) and we know several strong astrophysical candidates [1]. In 4-dimensional General Relativity, an uncharged BH is described by the Kerr solution and it is completely characterized by two quantities, the mass M and the spin parameter $a_* = J/M^2$, where J is the BH spin angular momentum [2]¹. A fundamental limit for a 4-dimensional Kerr BH is the bound $|a_*| \leq 1$, which is the condition for the existence of the event horizon. For $|a_*| > 1$, there is no horizon and the Kerr metric describes the gravitational field of a naked singularity, which is forbidden by the Weak Cosmic Censorship Conjecture [3].

The study of the orbital motion of individual stars around a BH candidate can provide robust measurements of the mass of the latter: these stars are typically far from the compact object and one can estimate M by using Newtonian mechanics, with no assumptions about the nature of the BH candidate. On the contrary, the measurement of the spin is much more challenging. The spin has no effects in Newtonian gravity and it can be estimated only probing the space-time close to the compact object. That can be potentially achieved by studying the properties of the electromagnetic radiation emitted by the gas of the accretion disk. The two most popular techniques to try to estimate a_* are the continuum-fitting

method [4] and the analysis of the broad $K\alpha$ iron line [5]. In both the approaches, an important assumption is that the inner edge of the disk is at the innermost stable circular orbit (ISCO). Since in the Kerr background there is a one-to-one correspondence between the ISCO radius and the spin parameter a_* , fitting the data we can get an estimate of a_* , supposing that all the astrophysical effects are well understood and properly taken into account.

As there is not yet clear evidence that the geometry of the space-time around BH candidates is the one described by the Kerr solution, different authors have proposed different ways to test this hypothesis. The first proposal was put forward by Ryan, who suggested observing the gravitational waves emitted by an extreme-mass ratio inspiral (EMRI), i.e. a system consisting of a stellar-mass compact object orbiting around a super-massive BH candidate [6]: as future space-based gravitational wave detectors will be able to observe $\sim 10^4 - 10^6$ gravitational wave cycles emitted by an EMRI while the stellar-mass body is inspiraling into the gravitational field of the super-massive object, even a small deviation from the Kerr geometry will build up an observable dephasing in the gravitational waveforms, thus allowing one to map the space-time of the super-massive BH candidate with very high accuracy [7]. Besides tests based on gravitational waves, the space-time geometry around BH candidates can be probed even by very accurate observations of the orbital motion of stars. In the case of a stellar-mass BH candidate in an X-ray binary system, that is possible if the companion star is a radio pulsar [8]. In the case of the super-massive BH candidate at the center of our Galaxy, that might be achieved by monitoring stars orbiting at milliparsec distances from the compact

* bambi@fudan.edu.cn

¹ Throughout the paper, I use units in which $G_N = c = 1$, unless stated otherwise.

object [9].

Recently, there has been new interest in the subject [10–22], especially thanks to significant progress in the understanding of the properties of the electromagnetic radiation emitted by the gas in the accretion disk and to near future high-resolution sub-millimeter VLBI experiments. It has been shown that the continuum-fitting method [10, 11] and the analysis of the broad $K\alpha$ iron line [16] can be easily generalized to non-Kerr space-times and be used to test the Kerr-nature of astrophysical BH candidates. Unlike other proposals, the two techniques can be applied to already available X-ray data and therefore they are both of particular interest. The continuum-fitting method is based on the analysis of the thermal spectrum of a geometrically thin accretion disk and it can be applied only to stellar-mass BH candidates – in the case of super-massive BH candidates, the thermal spectrum falls in the UV range and dust absorption makes accurate measurements impossible. However, the fit of the disk’s thermal spectrum actually measures the radiative efficiency of the Novikov-Thorne model, $\eta = 1 - E_{\text{ISCO}}$, where E_{ISCO} is the specific energy of a test-particle at the ISCO radius [10, 12]. In other words, the thermal spectrum of the disk around a Kerr BH with spin a_* and radiative efficiency η is extremely similar, and eventually indistinguishable, from the one around a non-Kerr object with different spin parameter but same radiative efficiency.

The analysis of the broad $K\alpha$ iron line is based on some more subtle assumptions, but it is thought to be potentially a more powerful approach to probe the space-time geometry around BH candidates. A preliminary study for using the broad $K\alpha$ iron line to test the nature of astrophysical BH candidates has been presented in Ref. [16]. The aim of the present paper is to extend that work. I compare the $K\alpha$ iron line produced around a Kerr BH with the one generated around more generic objects. As already found in Ref. [16], there is a strong correlation between the spin and the deformation parameter. I consider several specific cases, covering a wide range of spins and inclination angles. The results are reported in Tab. I. It is also interesting to note that even a quite deformed object can provide a $K\alpha$ line similar to the one expected in a Kerr background, as is shown by the reduced χ^2 in the top right panel of Fig. 9. Despite that, the technique can still put an interesting bound on possible deviations from the Kerr geometry, independently of the value of a_* and without additional measurements, which, in general, is not the case for the continuum-fitting method.

The content of the present paper is as follows. In Section II, I review the analysis of the $K\alpha$ iron line in the Kerr background. In Section III, I consider the non-Kerr metric proposed in [23] and I extend the analysis of Ref. [16] to use the $K\alpha$ line to constrain the space-time geometry around an astrophysical BH candidate. I cover a wide range of spins and inclinations. In Section IV, I discuss the results of Section III, pointing out the differences with the continuum-fitting method and showing

the outcome of a possible combination of the two techniques. Summary and conclusions are in Section V.

II. BROAD $K\alpha$ IRON LINE IN THE KERR BACKGROUND

The X-ray spectrum of both stellar-mass and super-massive BH candidates is usually characterized by the presence of a power-law component. This feature is commonly interpreted as the inverse Compton scattering of thermal photons by electrons in a hot corona above the accretion disk. The geometry of the corona is not known and several models have been proposed. Such a “primary component” irradiates also the accretion disk, producing a “reflection component” in the X-ray spectrum. The illumination of the cold disk by the primary component also produces spectral lines by fluorescence. The strongest line is the $K\alpha$ iron line at 6.4 keV. This line is intrinsically narrow in frequency, while the one observed appears broadened and skewed. The interpretation is that the line is strongly altered by special and general relativistic effects, which produce a characteristic profile first predicted in Ref. [24] and then observed for the first time in the ASCA data of the Seyfert 1 galaxy MCG-6-30-15 [25]. In the specific case of MCG-6-30-15, this line is extraordinarily stable, in spite of a substantial variability of the continuum, suggesting that the analysis of its shape can be used to probe the geometry of the space-time around the BH candidate. It should be borne in mind, however, that the relativistic origin of the observed broad $K\alpha$ iron lines is not universally accepted, and some authors have proposed different explanations [26].

Within the interpretation of a relativistically broadened $K\alpha$ iron line, the shape of the line is primarily determined by the background metric, the geometry of the emitting region, the disk emissivity, and the disk’s inclination angle with respect to the line of sight of the distant observer [24]. In the standard framework of a Kerr background, M sets the length of the system, so everything scales as M or as some power of M , without affecting the shape of the line. The only relevant parameter of the background geometry is thus the spin a_* . In those sources for which there is indication that the $K\alpha$ iron line is mainly emitted close to the compact object, the emission region may be thought to range from the ISCO radius, $r_{\text{in}} = r_{\text{ISCO}}$, to some outer radius r_{out} . However, even more complicated geometries have been proposed, see e.g. Ref. [27]. In principle, the disk emissivity may be theoretically calculated. In practice, that is not feasible at present. The simplest choice is an intensity profile $I_e \propto r^\alpha$, with $\alpha < 0$ a free parameter to be determined during the fitting procedure. The fourth parameter is the inclination of the disk with respect to the line of sight of the distant observer, i . The dependence of the Kerr iron line profile on a_* , i , α , and r_{out} and summarized in this section has been analyzed in detail by many authors, starting with Ref. [24].

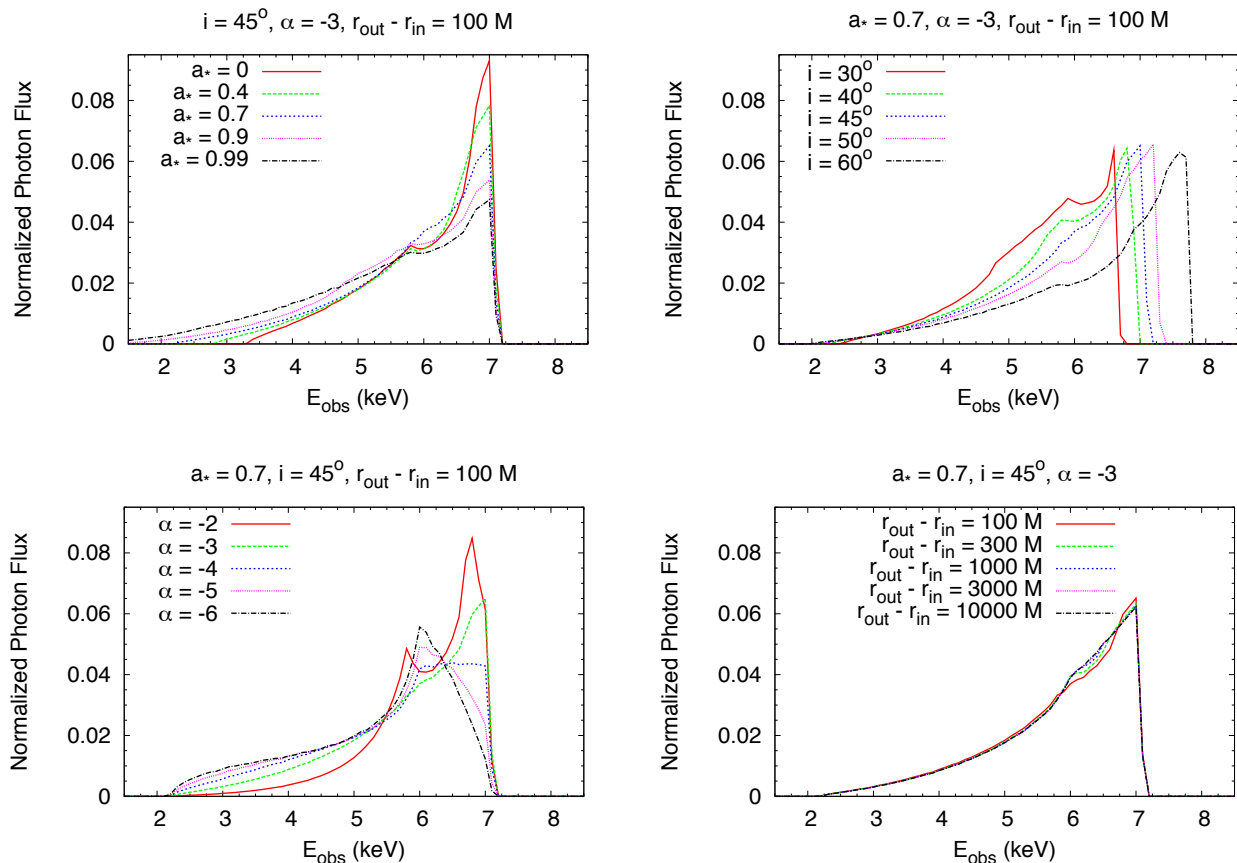


FIG. 1. Broad $K\alpha$ iron line in the Kerr background for different values of the parameters of the model. *Top left panel:* effect of the spin parameter a_* for a viewing angle $i = 45^\circ$, intensity profile with index $\alpha = -3$, and emissivity region $r_{\text{out}} - r_{\text{in}} = 100 M$. *Top right panel:* effect of the viewing angle for a spin parameter $a_* = 0.7$, intensity profile with index $\alpha = -3$, and emissivity region $r_{\text{out}} - r_{\text{in}} = 100 M$. *Bottom left panel:* effect of the intensity profile index α , for a spin parameter $a_* = 0.7$, viewing angle $i = 45^\circ$, and emissivity region $r_{\text{out}} - r_{\text{in}} = 100 M$. *Bottom right panel:* effect of the emissivity region for a spin parameter $a_* = 0.7$, viewing angle $i = 45^\circ$, and intensity profile with index $\alpha = -3$. See the text for details.

In what follows, I use the ray-tracing code described in [11]. The photon flux number density as measured by a distant observer is given by

$$\begin{aligned} N_{E_{\text{obs}}} &= \frac{1}{E_{\text{obs}}} \int I_{\text{obs}}(E_{\text{obs}}) d\Omega_{\text{obs}} = \\ &= \frac{1}{E_{\text{obs}}} \int g^3 I_e(E_e) d\Omega_{\text{obs}}. \end{aligned} \quad (1)$$

where I_{obs} and E_{obs} are, respectively, the specific intensity of the radiation and the photon energy as measured by the distant observer, $d\Omega_{\text{obs}}$ is the element of the solid angle subtended by the image of the disk on the observer's sky, I_e and E_e are, respectively, the local specific intensity of the radiation and the photon energy in the rest frame of the emitter, and $g = E_{\text{obs}}/E_e$ is the redshift factor. $I_{\text{obs}} = g^3 I_e$ follows from the Liouville's theorem. Unlike Ref. [11], here I assume that the disk emission is monochromatic (the rest frame energy is $E_{K\alpha} = 6.4$ keV) and isotropic with a power-law radial profile:

$$I_e(E_e) \propto \delta(E_e - E_{K\alpha}) r^\alpha. \quad (2)$$

The resulting broad $K\alpha$ iron lines for different values of the model parameters (spin a_* , inclination angle i , power-law index α , and outer radius r_{out}) are shown in Fig. 1. The photon flux has been normalized so that

$$\int N_{E_{\text{obs}}} dE_{\text{obs}} = \text{constant}, \quad (3)$$

as only the shape matters. The spin (left top panel) can be determined by the low-energy tail: a higher spin implies an inner radius closer to the compact object and therefore a larger fraction of photon is affected by a strong gravitational redshift ($r_{\text{ISCO}}/M = 6$ for $a_* = 0$ and monotonically goes to 1 for $a_* = 1$). The disk's inclination angle i (right top panel) moves the blue-shifted part of the spectrum: for small inclination angles, the Doppler boosting is not relevant, while for large inclination angles it becomes more and more important. The power-law index α (left bottom panel) balances the importance of the emission in the innermost region with respect to the one at larger radii. For high values of α , e.g. $\alpha = -2$, the contribution of the emission at relatively

large radii is significant, so the Doppler blue-shifted part of the spectrum results in a prominent peak, while the gravitational red-shifted part has a lower flux. For lower and lower values of α , the photon flux in the Doppler blue-shifted part of the spectrum decreases, while the one in the gravitational red-shifted part increases. Lastly, the position of the outer radius of the emission region r_{out} (right bottom panel) changes the position of the low energy peak of the spectrum, although the effect is small for $\alpha = -3$ or lower.

III. BROAD $K\alpha$ IRON LINE IN A NON-KERR BACKGROUND

In order to test the Kerr-nature of astrophysical BH candidates, it is convenient to adopt the following approach (see the first paper in [17]). We consider a background more general than the Kerr metric, which includes the Kerr solution as a special case. In the simplest scenario, we consider a metric specified by a mass M , spin parameter a_* and a single deformation parameter

$$ds^2 = - \left(1 - \frac{2Mr}{\Sigma}\right) (1+h) dt^2 + \frac{\Sigma(1+h)}{\Delta + a^2 h \sin^2 \theta} dr^2 + \Sigma d\theta^2 - \frac{4aMr \sin^2 \theta}{\Sigma} (1+h) dt d\phi + \left[\sin^2 \theta \left(r^2 + a^2 + \frac{2a^2 Mr \sin^2 \theta}{\Sigma} \right) + \frac{a^2 (\Sigma + 2Mr) \sin^4 \theta}{\Sigma} h \right] d\phi^2, \quad (4)$$

where $a = a_* M$, $\Sigma = r^2 + a^2 \cos^2 \theta$, $\Delta = r^2 - 2Mr + a^2$, and

$$h = \sum_{k=0}^{\infty} \left(\epsilon_{2k} + \frac{Mr}{\Sigma} \epsilon_{2k+1} \right) \left(\frac{M^2}{\Sigma} \right)^k. \quad (5)$$

This metric has an infinite number of deformation parameters ϵ_i and the Kerr solution is recovered when all the deformation parameters are set to zero. However, in order to reproduce the correct Newtonian limit, we have to impose $\epsilon_0 = \epsilon_1 = 0$, while ϵ_2 is strongly constrained by Solar System experiments [23]. In this paper, I will

measuring possible deviations from the Kerr background. The idea is then to compute the properties of the radiation emitted by the accretion disk (in our case the shape of the $K\alpha$ iron line) in this new background and check if observations demand a vanishing deformation parameter; that is, the Kerr BH hypothesis is confirmed.

The approach is clearly quite phenomenological, in the sense that we do not aim at testing a specific and self-consistent gravity theory, but we use a metric as generic as possible with a deformation that, as a first approximation, is used to quantify possible deviations from the Kerr background. The approach makes sense because in the end we want to perform a null-experiment: we have a deformation parameter and we want to check that it must vanish, i.e. the compact object is a Kerr BH, regardless of the physical meaning of a non-zero deformation parameter. With this spirit, here I consider the Johannsen-Psaltis (JP) metric, which can be seen as a metric describing non-Kerr BHs in a putative alternative theory of gravity [23]. In Boyer-Lindquist coordinates, the JP metric is given by the line element

only examine the simplest cases where $\epsilon_3 \neq 0$, while all the other deformation parameters are set to zero.

The effects of a non-vanishing ϵ_3 on the shape of the $K\alpha$ iron line have been discussed in Ref. [16] and are summarized in Fig. 2. The deformation parameter ϵ_3 changes the spectrum of the line in a way similar to the spin parameter a_* , while i , α , and r_{out} seem to produce different deformations. In order to be more quantitative, we can compare the line produced in a Kerr space-time with the one expected from a JP background. That can be done as in Ref. [10], by defining the reduced χ^2 :

$$\chi_{\text{red}}^2(a_*, \epsilon_3, i, \alpha, r_{\text{out}}) = \frac{\chi^2}{n} = \frac{1}{n} \sum_{i=1}^n \frac{[N_i^{\text{JP}}(a_*, \epsilon_3, i, \alpha, r_{\text{out}}) - N_i^{\text{Kerr}}(\tilde{a}_*, \tilde{i}, \tilde{\alpha}, \tilde{r}_{\text{out}})]^2}{\sigma_i^2}, \quad (6)$$

where the summation is performed over n sampling energies E_i and N_i^{JP} and N_i^{Kerr} are the normalized photon fluxes in the energy bin $[E_i, E_i + \Delta E]$ respectively for the JP and Kerr metric. Here the error σ_i is assumed to be

15% the normalized photon flux N_i^{Kerr} :

$$\sigma_i = 0.15 N_i^{\text{Kerr}}. \quad (7)$$

As a first example, we can consider the line produced around a mid-rotating Kerr BH with $\tilde{a}_* = 0.70$. Within a simplified analysis, we can assume $i = \tilde{i}$, $\alpha = \tilde{\alpha}$, and

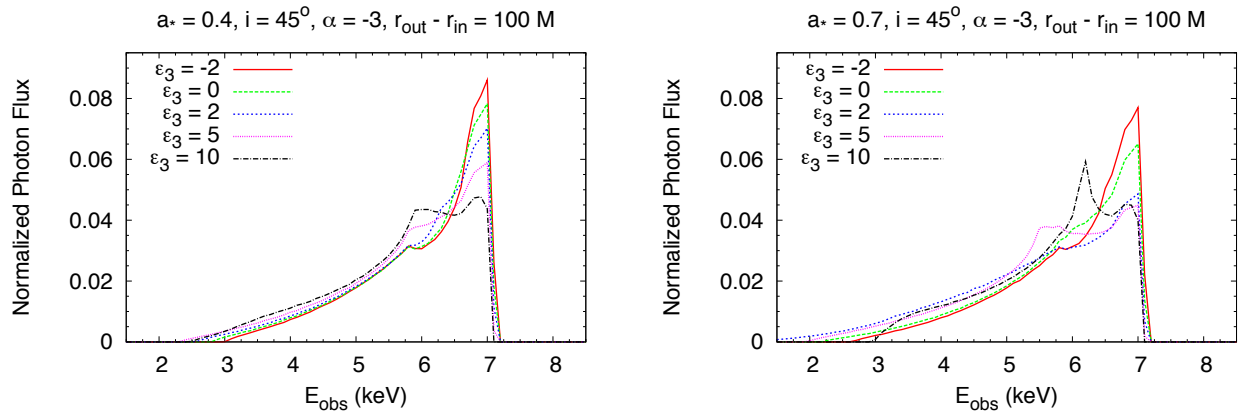


FIG. 2. Broad $K\alpha$ iron line in the JP background for different values of the deformation parameter ϵ_3 . *Left panel*: spin parameter $a_* = 0.4$. *Right panel*: spin parameter $a_* = 0.7$. In both the panels, the viewing angle is $i = 45^\circ$, the intensity profile index is $\alpha = -3$, and the emissivity region is $r_{\text{out}} - r_{\text{in}} = 100 M$. See the text for details.

$r_{\text{out}} - r_{\text{in}} = \tilde{r}_{\text{out}} - \tilde{r}_{\text{in}}$ and make a_* and ϵ_3 change. This is the approach adopted in Ref. [16] and the motivation is that i , α and r_{out} produce different effects on the shape of the line with respect to a_* and ϵ_3 and therefore the determination of the former from the fit is relatively independent of the measurement of the latter. Fig. 3 shows the reduced χ^2 for $\tilde{i} = 45^\circ$ (top left panel), $\tilde{i} = 15^\circ$ (central left panel), and $\tilde{i} = 75^\circ$ (bottom left panel). The $1-\sigma$ bound on a_* and ϵ_3 ($\chi_{\text{red}}^2 < 1$) is reported in Tab. I. If we relax the assumption $i = \tilde{i}$, we get the plots in the right column. The corresponding $1-\sigma$ is clearly weaker, as shown in Tab. I. The difficulty of constraining ϵ_3 without an independent measurement of the spin parameter a_* was already pointed out in Ref. [16].

If we change the value of the spin parameter of the reference spectrum, we can find the plots in Figs. 4 and 5. Fig. 4 shows the cases $\tilde{a}_* = 0.20$ (top panels) and 0.92 (bottom panels), for $\tilde{i} = i = 45^\circ$ (left panels) and $\tilde{i} = 45^\circ$ and i free (right panels). Fig. 5 shows instead the case $\tilde{a}_* = 0.98$ with $\tilde{i} = 45^\circ$ (top panels), $\tilde{i} = 15^\circ$ (central panels), and $\tilde{i} = 75^\circ$ (bottom panels), assuming either $\tilde{i} = i$ (left panels) or with i as a free parameter (right panels). The $1-\sigma$ bounds for these cases are reported in Tab. I.

Effects of variations of the index parameter α may also be important. Fig. 6 shows the comparison of the iron line profile of a Kerr BH with $\tilde{a}_* = 0.70$ with the one of a JP BH with spin a_* and deformation parameter ϵ_3 . In this case, I impose $i = \tilde{i}$ and $r_{\text{out}} - r_{\text{in}} = \tilde{r}_{\text{out}} - \tilde{r}_{\text{in}}$, while $\tilde{\alpha} = -3$ but α is free. The $1-\sigma$ bound is only a little bit more stringent than the case with $\tilde{\alpha} = \alpha$ and i arbitrary. The effect of an unknown \tilde{r}_{out} is important for $\alpha = -2$ and $\tilde{r}_{\text{out}} - \tilde{r}_{\text{in}} \approx 10 M$, but becomes less and less relevant for lower values of the index of the intensity profile and larger \tilde{r}_{out} .

IV. DISCUSSION

A. Constraints on the spin parameter-deformation parameter plane

In the Kerr background, the exact value of the spin parameter sets the inner edge of the accretion disk. The radiation emitted from the region closer to the BH candidate is more gravitationally redshifted and for this reason a_* can be estimated by studying the low-energy tail of the broad $K\alpha$ iron line. On the other hand, the Keplerian velocity profile depends very weakly on the spin parameter. The high-energy peak of the line is produced by the Doppler boosting from radiation emitted at relatively large radii; indeed, if the emissivity at large radii is strongly suppressed the high-energy peak disappears (e.g. for $\alpha \lesssim -4$, see the left bottom panel of Fig. 1). The position of the high-energy peak is thus determined by the inclination angle of the disk with respect to the observer's line of sight. In the Kerr space-time, the spin parameter and the inclination angle can be determined by two different parts of the relativistically broadened line and the two measurements are not correlated.

If we consider the possibility of a non-vanishing deformation parameter, the picture is different. In the case of the JP background discussed in the previous section, the effect of a small ϵ_3 is very similar to a variation of the spin parameter a_* ; that is, ϵ_3 alters the low-energy tail of the line and it is not possible to distinguish a line emitted around a Kerr BH with the one coming from a non-Kerr compact object with a different spin parameter. However, for larger deviations from the Kerr geometry, the variation of the Keplerian velocity profile also becomes relevant. That has two effects. First, the distortion produced by a_* and ϵ_3 are not equivalent any more and it is possible to get a bound on possible deviations from Kerr independently of the value of the spin parameter. For instance, in the case of the thermal spectrum of the

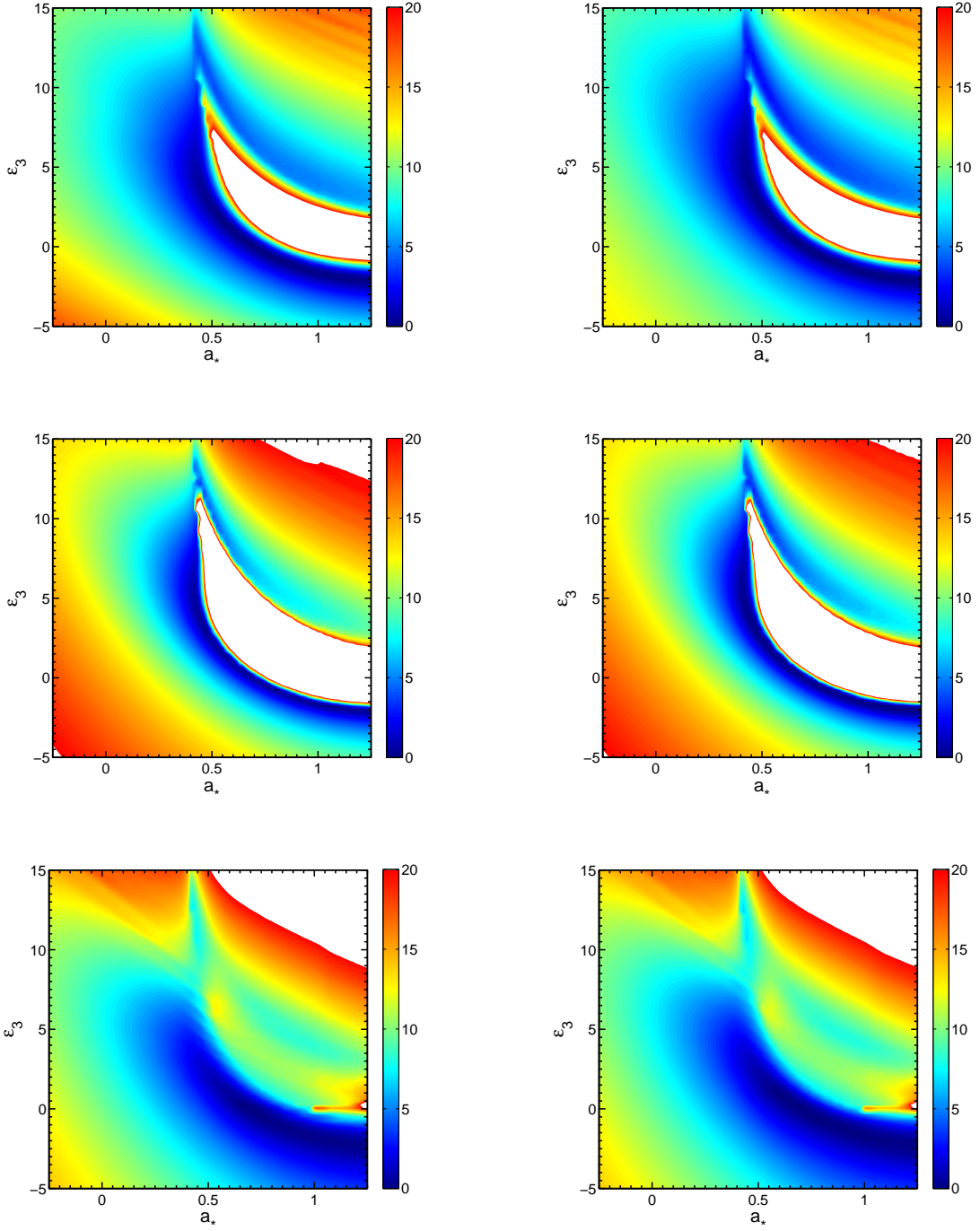


FIG. 3. χ_{red}^2 from the comparison of the broad $\text{K}\alpha$ iron line produced in a Kerr space-time with spin parameter $\tilde{a}_* = 0.70$ and the one in a JP space-time with spin parameter a_* and deformation parameter ϵ_3 . *Top left panel:* $\tilde{i} = i = 45^\circ$. *Top right panel:* $\tilde{i} = 45^\circ$ and i free. *Central left panel:* $\tilde{i} = i = 15^\circ$. *Central right panel:* $\tilde{i} = 15^\circ$ and i free. *Bottom left panel:* $\tilde{i} = i = 75^\circ$. *Bottom right panel:* $\tilde{i} = 75^\circ$ and i free. The other parameters of the model are $\tilde{\alpha} = \alpha = -3$ and $\tilde{r}_{\text{out}} - \tilde{r}_{\text{in}} = r_{\text{out}} - r_{\text{in}} = 100 M$. See the text for details.

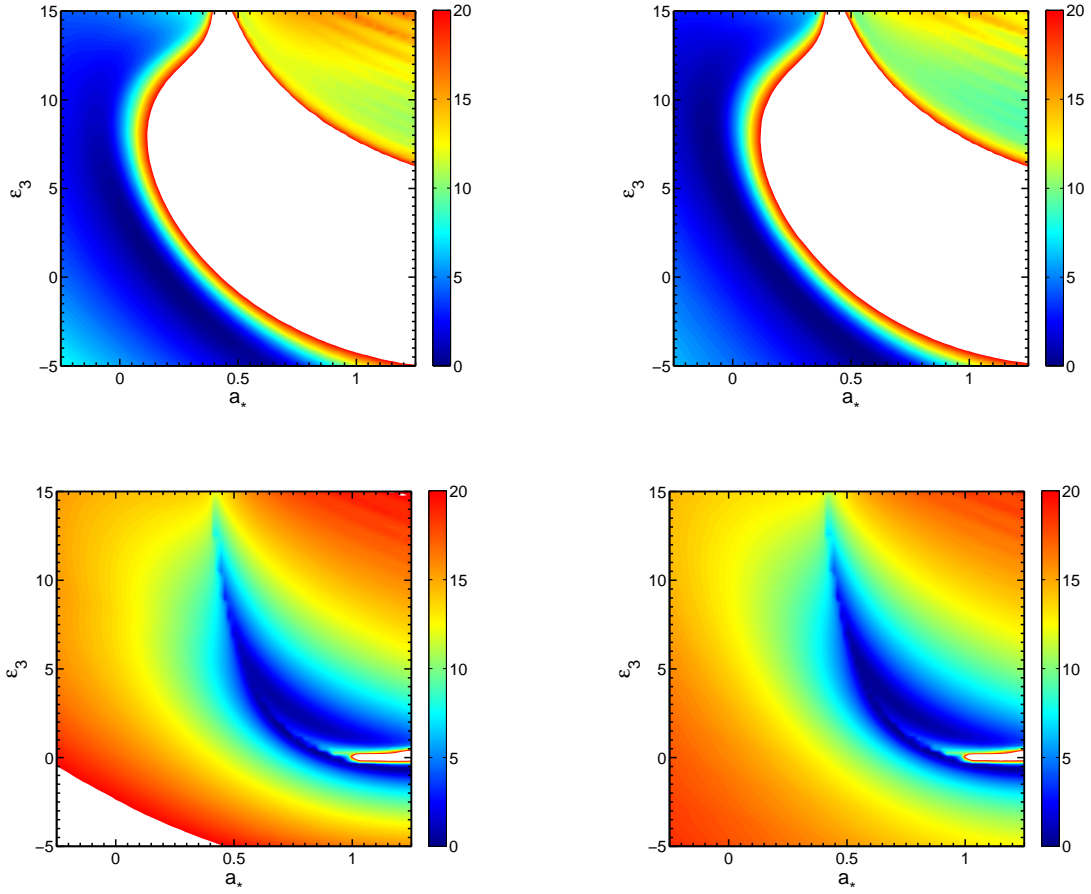


FIG. 4. χ_{red}^2 from the comparison of the broad $\text{K}\alpha$ iron line produced in a Kerr space-time with spin parameter \tilde{a} and the one in a JP space-time with spin parameter a_* and deformation parameter ϵ_3 . *Top left panel:* $\tilde{a}_* = 0.20$ and $\tilde{i} = i = 45^\circ$. *Top right panel:* $\tilde{a}_* = 0.20$, $\tilde{i} = 45^\circ$, and i free. *Bottom left panel:* $\tilde{a}_* = 0.92$ and $\tilde{i} = i = 45^\circ$. *Bottom right panel:* $\tilde{a}_* = 0.92$, $\tilde{i} = 45^\circ$, and i free. See the text for details.

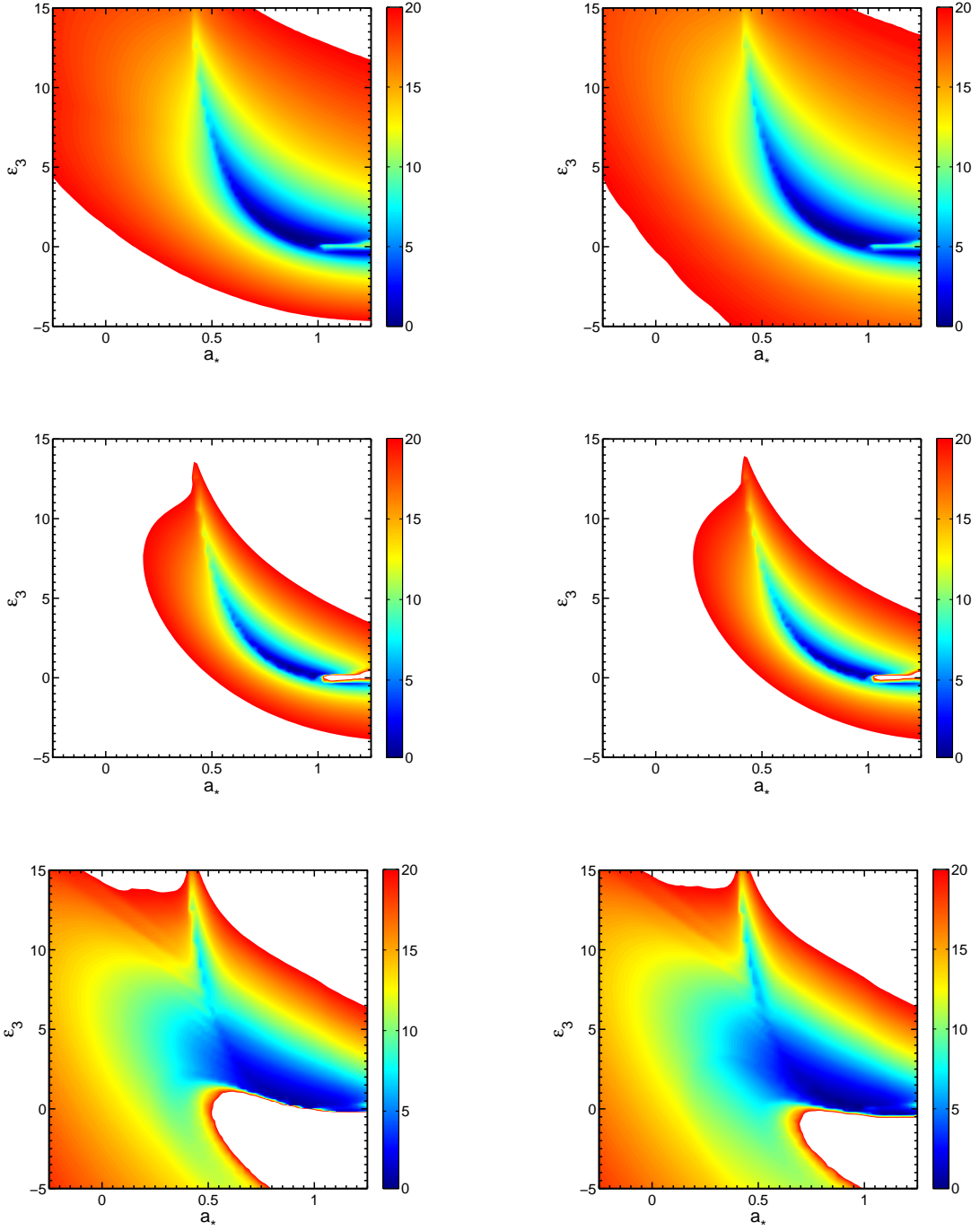


FIG. 5. χ_{red}^2 from the comparison of the broad $\text{K}\alpha$ iron line produced in a Kerr space-time with spin parameter $\tilde{a}_* = 0.98$ and the one in a JP space-time with spin parameter a_* and deformation parameter ϵ_3 . *Top left panel:* $\tilde{i} = i = 45^\circ$. *Top right panel:* $\tilde{i} = 45^\circ$ and i free. *Central left panel:* $\tilde{i} = i = 15^\circ$. *Central right panel:* $\tilde{i} = 15^\circ$ and i free. *Bottom left panel:* $\tilde{i} = i = 75^\circ$. *Bottom right panel:* $\tilde{i} = 75^\circ$ and i free. The other parameters of the model are $\tilde{\alpha} = \alpha = -3$ and $\tilde{r}_{\text{out}} - \tilde{r}_{\text{in}} = r_{\text{out}} - r_{\text{in}} = 100 M$. See the text for details.

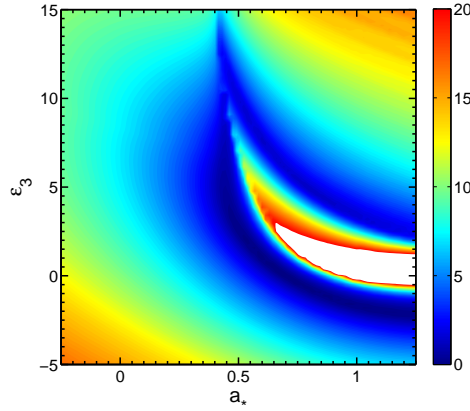


FIG. 6. As in Fig. 3 for $\tilde{i} = i = 45^\circ$, $\tilde{\alpha} = -3$, and α free

Reference spectrum	Model	Kerr background	JP background
Kerr with $a_* = 0.70$	$\tilde{i} = 45^\circ$	$a_* = 0.70 \pm 0.05$	$a_* > 0.41, \epsilon_3 < 5.3$
	$\tilde{i} = 45^\circ, i$ free	$a_* = 0.70 \pm 0.05$	$a_* > 0.39, \epsilon_3 < 7.3$
	$\tilde{i} = 45^\circ, \alpha$ free	$a_* = 0.70 \pm 0.06$	$a_* > 0.41, \epsilon_3 < 7.0$
	$\tilde{i} = 15^\circ$	$a_* = 0.70^{+0.02}_{-0.03}$	$a_* > 0.41, \epsilon_3 < 6.7$
	$\tilde{i} = 15^\circ, i$ free	$a_* = 0.70 \pm 0.03$	$a_* > 0.39, \epsilon_3 < 7.8$
	$\tilde{i} = 75^\circ$	$a_* = 0.70 \pm 0.09$	$a_* > 0.53, \epsilon_3 < 1.8$
	$\tilde{i} = 75^\circ, i$ free	$a_* = 0.70 \pm 0.09$	$a_* > 0.48, \epsilon_3 < 2.6$
	$\tilde{i} = 45^\circ, \text{CFM}$	$a_* = 0.70^{+0.03}_{-0.05}$	no bound
	$\tilde{i} = 45^\circ, \text{CFM}+\text{K}\alpha$	$a_* = 0.70 \pm 0.03$	$0.45 < a_* < 1.14, -2.3 < \epsilon_3 < 2.8$
Kerr with $a_* = 0.20$	$\tilde{i} = 45^\circ$	$a_* = 0.20^{+0.05}_{-0.10}$	$a_* > -0.12, \epsilon_3 < 7.4$
	$\tilde{i} = 45^\circ, i$ free	$a_* = 0.20^{+0.05}_{-0.10}$	$a_* > -0.18, \epsilon_3 < 11.6$
Kerr with $a_* = 0.92$	$\tilde{i} = 45^\circ$	$a_* = 0.92^{+0.03}_{-0.04}$	$a_* > 0.53, \epsilon_3 < 5.6$
	$\tilde{i} = 45^\circ, i$ free	$a_* = 0.92^{+0.03}_{-0.04}$	$a_* > 0.49, \epsilon_3 < 7.3$
Kerr with $a_* = 0.98$	$\tilde{i} = 45^\circ$	$a_* = 0.98^{+0.01}_{-0.03}$	$a_* > 0.65, \epsilon_3 < 2.6$
	$\tilde{i} = 45^\circ, i$ free	$a_* = 0.98^{+0.01}_{-0.03}$	$a_* > 0.63, \epsilon_3 < 3.1$
	$\tilde{i} = 15^\circ$	$a_* = 0.98 \pm 0.01$	$0.71 < a_* < 1.10, -0.2 < \epsilon_3 < 1.8$
	$\tilde{i} = 15^\circ, i$ free	$a_* = 0.98 \pm 0.01$	$0.71 < a_* < 1.15, -0.3 < \epsilon_3 < 1.8$
	$\tilde{i} = 75^\circ$	$a_* = 0.98 \pm 0.01$	$a_* > 0.77, \epsilon_3 < 1.2$
	$\tilde{i} = 75^\circ, i$ free	$a_* = 0.98^{+0.01}_{-0.07}$	$a_* > 0.74, \epsilon_3 < 1.5$
	$\tilde{i} = 45^\circ, \text{CFM}$	$a_* = 0.98^{+0.01}_{-0.02}$	$a_* > 0.44, \epsilon_3 < 12.4$
$\tilde{i} = 45^\circ, \text{CFM}+\text{K}\alpha$	$a_* = 0.98 \pm 0.01$	$0.70 < a_* < 1.10, -0.4 < \epsilon_3 < 2.2$	

TABLE I. $1\text{-}\sigma$ bounds on the spin parameter a_* (in the Kerr background) and on the spin parameter-deformation parameter plane (in the JP background) for the cases shown in Figs. 3-8. Unless stated otherwise, $\tilde{i} = i$, $\tilde{\alpha} = \alpha = -3$, and $\tilde{r}_{\text{out}} - \tilde{r}_{\text{in}} = r_{\text{out}} - r_{\text{in}} = 100 M$. CFM stands for continuum-fitting method, while CFM+K α is the case in which the measurements from the continuum-fitting method and the K α iron line are combined. In this paper, I studied only the region $-0.25 < a_* < 1.25$ and $-5 < \epsilon_3 < 15$ of the spin-deformation parameter plane; the expression “no bound” in the table means that at $1\text{-}\sigma$ it is not possible to exclude any value of the spin in the range $-0.25 < a_* < 1.25$, as well as any value of the deformation parameter in the range $-5 < \epsilon_3 < 15$.

Reference spectrum	Model	$\epsilon_3 = 7.0$ JP background	JP background
JP with $a_* = 0.20$, $\epsilon_3 = 7.0$	$\tilde{i} = 45^\circ$	$a_* = 0.20 \pm 0.05$	$0.15 < a_* < 0.25$, $6.3 < \epsilon_3 < 8.8$
	$\tilde{i} = 45^\circ$, i free	$a_* = 0.20 \pm 0.05$	$0.15 < a_* < 0.86$, $\epsilon_3 < 11.2$
	$\tilde{i} = 45^\circ$, CFM	$a_* = 0.20^{+0.03}_{-0.04}$	no bound
	$\tilde{i} = 45^\circ$, CFM+K α	$a_* = 0.20 \pm 0.03$	$0.17 < a_* < 0.24$, $6.3 < \epsilon_3 < 7.7$

TABLE II. As in Tab. I for the cases shown in Fig. 9, in which the reference metric has $a_* = 0.20$ and $\epsilon_3 = 7.0$.

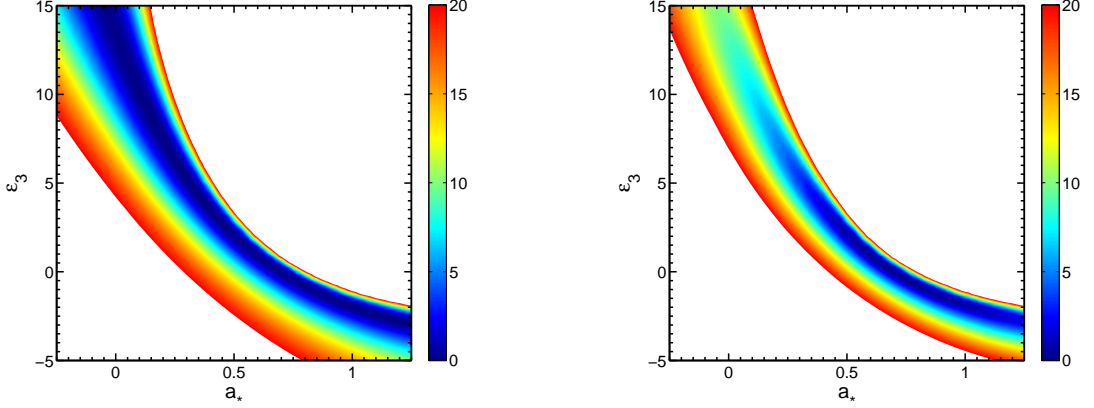


FIG. 7. *Left panel:* χ_{red}^2 from the comparison of the thermal spectrum of a thin accretion disk around a Kerr BH with spin parameter $\tilde{a}_* = 0.70$ and the one in a JP space-time with spin parameter a_* and deformation parameter ϵ_3 . *Right panel:* $\chi_{\text{red,tot}}^2$ from the combination of the analysis of the broad K α iron line and the continuum-fitting method. The parameters of the model are: mass $M = 10 M_\odot$, mass accretion rate $\dot{M} = 2 \cdot 10^{18} \text{ g s}^{-1}$, distance $D = 10 \text{ kpc}$, and viewing angle $i = 45^\circ$. See the text for details.

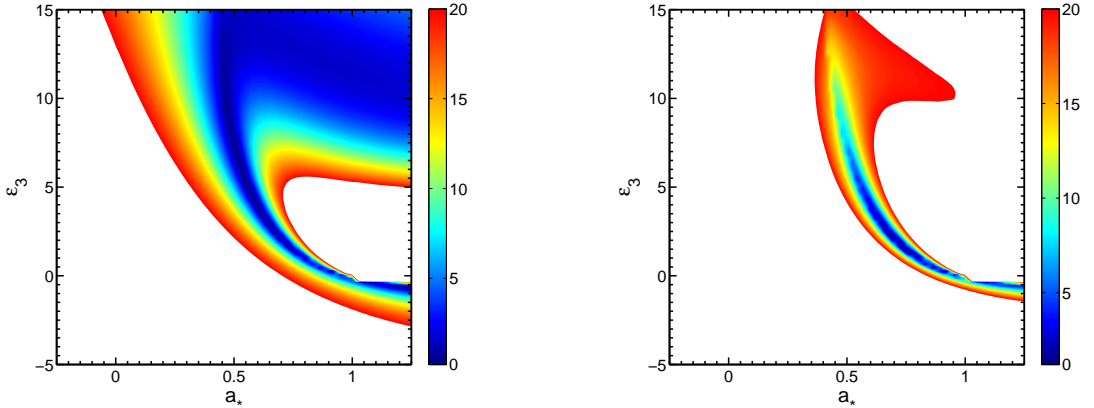


FIG. 8. *Left panel:* χ_{red}^2 from the comparison of the thermal spectrum of a thin accretion disk around a Kerr BH with spin parameter $\tilde{a}_* = 0.98$ and the one in a JP space-time with spin parameter a_* and deformation parameter ϵ_3 . *Right panel:* $\chi_{\text{red,tot}}^2$ from the combination of the analysis of the broad K α iron line and the continuum-fitting method. The parameters of the model are: mass $M = 10 M_\odot$, mass accretion rate $\dot{M} = 2 \cdot 10^{18} \text{ g s}^{-1}$, distance $D = 10 \text{ kpc}$, and viewing angle $i = 45^\circ$. See the text for details.

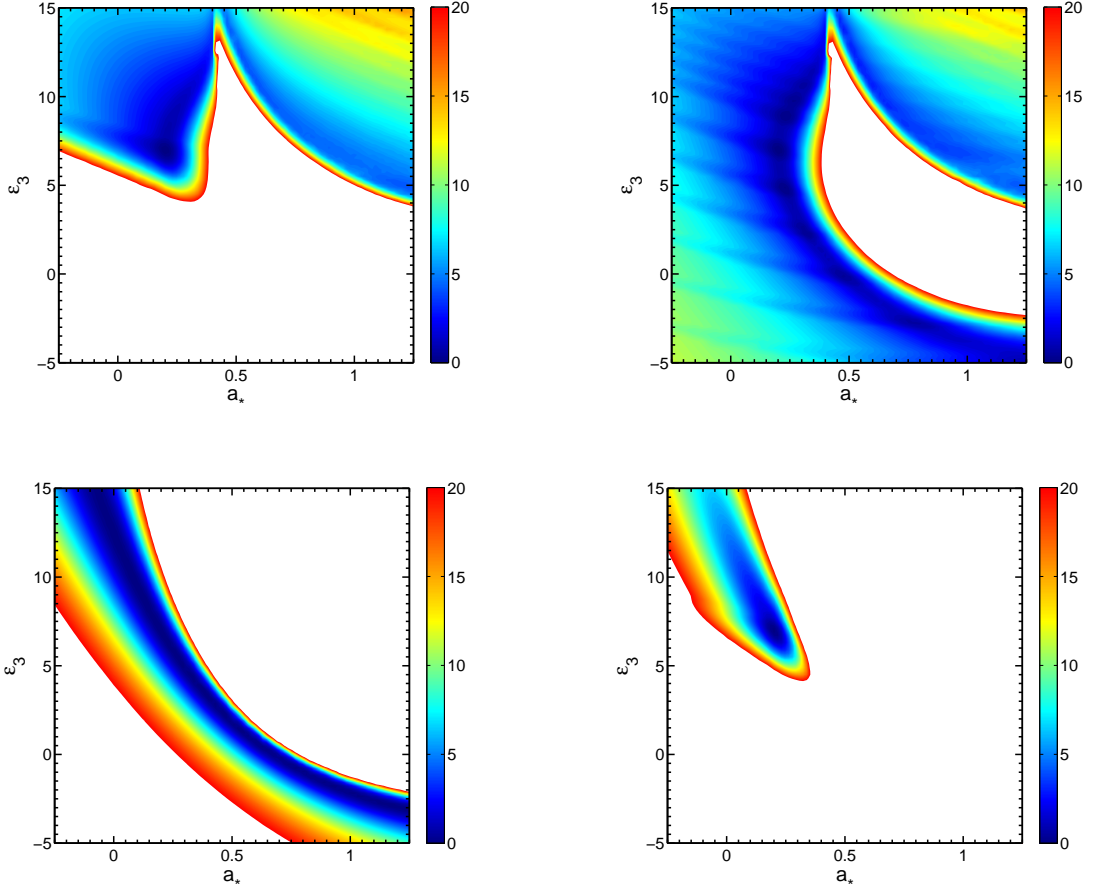


FIG. 9. *Top left panel:* χ_{red}^2 from the comparison of the broad $K\alpha$ iron line produced in a JP space-time with spin parameter $\tilde{a}_* = 0.20$ and $\tilde{\epsilon}_3 = 7.0$ and the one in a JP space-time with spin parameter a_* and deformation parameter ϵ_3 . $\tilde{i} = i = 45^\circ$. *Top right panel:* as in the left panel, for $\tilde{i} = 45^\circ$ and i free. *Bottom left panel:* χ_{red}^2 from the comparison of the thermal spectrum of a thin accretion disk around a JP BH with spin parameter $\tilde{a}_* = 0.20$ and $\tilde{\epsilon}_3 = 7.0$ and the one in a JP space-time with spin parameter a_* and deformation parameter ϵ_3 . The parameters of the model are: mass $M = 10 M_\odot$, mass accretion rate $\dot{M} = 2 \cdot 10^{18} \text{ g s}^{-1}$, distance $D = 10 \text{ kpc}$, and viewing angle $i = 45^\circ$. *Bottom right panel:* $\chi_{\text{red,tot}}^2$ from the combination of the analysis of the broad $K\alpha$ iron line and the continuum-fitting method. See the text for details.

disk, interesting bounds may not be possible (see next subsection). Second, the determination of a_* and ϵ_3 is not really independent of the measurement of the inclination angle i : for this reason, the fact the inclination angle has also to be determined by the fit increases the allowed region in the plane spin parameter-deformation parameter.

B. Comparison with the continuum-fitting method

It is interesting to compare the information on the space-time geometry present in the shape of the broad $K\alpha$ iron line with the one in the thermal spectrum of a thin accretion disk. The extension of the continuum-fitting method to non-Kerr space-times was discussed in Refs. [10, 11], where it was shown that this technique actually measures the radiative efficiency of the Novikov-Thorne model, $\eta = 1 - E_{\text{ISCO}}$. In other words, the approach cannot really distinguish the spectrum of a thin disk around a Kerr BH with spin parameter a_* and radiative efficiency η from the one in a non-Kerr space-time with completely different value of the spin parameter but same radiative efficiency. This simple rule was exploited in [12] to quickly get the allowed region on the spin parameter-deformation parameter plane of the stellar-mass BH candidates whose spin has been estimated under the assumption of the Kerr metric.

The thermal spectrum of a thin disk in the Kerr space-time depends on five parameters (mass of the BH candidate M , spin parameter a_* , mass accretion rate of the BH candidate \dot{M} , distance of the binary system D , and inclination angle of the disk i). M , D , and i should be deduced from independent measurements, while a_* and \dot{M} are inferred by fitting the disk's spectrum. However, a_* and \dot{M} are not correlated, as the former changes the position of the peak, while the latter changes the intensity of the low energy region of the spectrum. We can then define χ_{red}^2 with the same spirit of Section III and Ref. [10]

$$\chi_{\text{red}}^2(a_*, \epsilon_3) = \frac{1}{n} \sum_{i=1}^n \frac{[N_i^{\text{JP}}(a_*, \epsilon_3) - N_i^{\text{Kerr}}(\tilde{a}_*)]^2}{\sigma_i^2}, \quad (8)$$

and compare the disk's spectrum of a Kerr BH with the one of a JP space-time. The uncertainty σ_i is still assumed to be 15% the photon flux of the reference spectrum; i.e., $\sigma_i = 0.15 N_i^{\text{Kerr}}(\tilde{a}_*)$. Here the spectra have been computed with the code described in Ref. [11], assuming a mass accretion rate $\dot{M} = 2 \cdot 10^{18} \text{ g s}^{-1}$ and a viewing angle $i = 45^\circ$. Unlike the analysis of the broad iron line profile, in the continuum-fitting method the inclination angle i must be obtained from independent measurements and is an input parameter. The resulting χ_{red}^2 are shown in the left panels of Figs. 7 and 8, respectively for a spin parameter $\tilde{a}_* = 0.70$ and 0.98. The 1- σ constraints are reported in Tab. I. Especially for

$\tilde{a}_* = 0.70$, deviations from the Kerr background can be very large if we increase the difference of the value of a_* with respect to the Kerr case. At the same time, for small values of the deformation parameter ϵ_3 , the degeneracy between a_* and ϵ_3 in the continuum-fitting method and in the analysis of the broad $K\alpha$ iron line is very similar.

If we have a BH candidate for which we can get good data of the thermal spectrum of its accretion disk in the high-soft state and of the broad $K\alpha$ iron line, we can combine the two measurements. We can see the constraint we can obtain from the combinations of the two techniques by introducing $\chi_{\text{red,tot}}^2$, defined as

$$\chi_{\text{red,tot}}^2 = \chi_{\text{red,K}\alpha}^2 + \chi_{\text{red,cfm}}^2, \quad (9)$$

where $\chi_{\text{red,K}\alpha}^2$ and $\chi_{\text{red,cfm}}^2$ are, respectively, the reduced χ^2 from the analysis of the $K\alpha$ iron line, defined in Eq. (6), and of the thermal spectrum of a thin accretion disk, defined in Eq. (8). If we consider the case in which $\tilde{i} = i = 45^\circ$, $\tilde{\alpha} = \alpha = -3$, and $r_{\text{out}} - r_{\text{in}} = \tilde{r}_{\text{out}} - \tilde{r}_{\text{in}} = 100 M$, the $\chi_{\text{red,tot}}^2$ is the one shown in the right panel of Fig. 7 for $\tilde{a}_* = 0.70$ and in the right panel of Fig. 8 for $\tilde{a}_* = 0.98$. The 1- σ constraints are reported in Tab. I.

Lastly, we can consider the possibility that astrophysical BH candidates are not Kerr BHs and therefore that the reference spectrum is generated in a space-time with non-vanishing deformation parameter. χ_{red}^2 is now given by Eqs. (6) and (8) with N_i^{Kerr} replaced by $N_i^{\text{JP}}(\tilde{a}_*, \tilde{\epsilon}_3, \dots)$. Fig. 9 shows the results for the case with $\tilde{a}_* = 0.20$ and $\tilde{\epsilon}_3 = 7.0$. In the top left panel, there is the χ_{red}^2 from the $K\alpha$ iron line, assuming $\tilde{i} = i = 45^\circ$, $\tilde{\alpha} = \alpha = -3$, and $r_{\text{out}} - r_{\text{in}} = \tilde{r}_{\text{out}} - \tilde{r}_{\text{in}} = 100 M$. Here, if we try to fit the line profile with the one of a Kerr space-time, we should get a bad fit, at least if all the astrophysical processes are properly taken into account and one of the latter is not used to make the fit good. However, as i is also a fit parameter, the assumption $\tilde{i} = i$ is not justified. If we consider i as a free parameter, the picture changes dramatically. The reduced χ^2 from the iron line is now shown in the top right panel of Fig. 9 and it is perfectly consistent with a Kerr BH with spin $a_* \sim 0.5$. If we repeat the analysis of the disk's spectrum, we find the χ_{red}^2 in the left bottom panel of Fig. 9 and, combining the two techniques, we get the one in the right bottom panel. In the latter case, I have assumed $\tilde{i} = i$, since the continuum-fitting method needs in any case i as input parameter. However, we can note that the measurements from the iron line profile and the continuum-fitting method of the spin parameter assuming (incorrectly) that the object is a Kerr BH are not completely consistent. The analysis of the $K\alpha$ iron line would suggest $a_* = 0.47 \pm 0.04$. The continuum-fitting method would measure $a_* = 0.68_{-0.07}^{+0.03}$.

V. SUMMARY AND CONCLUSIONS

Astrophysical BH candidates are thought to be the Kerr BHs predicted by General Relativity, but the actual

nature of these objects has still to be verified. In order to confirm the Kerr BH hypothesis, we have to observe strong gravity features and check that they are consistent with the predictions of General Relativity. It turns out that one can do it by extending current techniques used to estimate (under the assumption of Kerr background) the spin of these objects. The continuum-fitting method and the analysis of the broad $K\alpha$ iron line are the two most robust approaches and they can already provide constraints on possible deviations from the Kerr geometry with the available X-ray data. These two features make the continuum-fitting method and the $K\alpha$ iron line analysis particularly interesting in comparison with other approaches discussed in the literature and possible only after the advent of future experiments.

In the present paper, I focused the attention on the analysis of the broad $K\alpha$ iron line, which is quite commonly seen in the X-ray spectrum of both stellar-mass and super-massive BH candidates and it is interpreted as the fluorescent lines produced by X-ray irradiation of the cold gas in the accretion disk. Here, I extended previous work in the literature. There is a significant correlation between spin parameter a_* , deformation parameter ϵ_3 , and the disk's inclination angle i . In the Kerr metric, the Keplerian velocity profile at relatively large radii is quite

independent of the exact value of the spin parameter and therefore the determinations of a_* and i from the shape of the line are not very much correlated. In the case of a non-Kerr space-time, the deformation parameter can affect the Keplerian velocity profile, with the result that a_* , ϵ_3 , and i are not independent any more and the constraint on possible deviations from the Kerr geometry becomes weaker. Despite that, the analysis of the broad $K\alpha$ iron line can potentially provide stronger bounds on ϵ_3 than the study of the thermal component of the accretion disk, as can be easily seen by checking Tabs. I and II (the continuum-fitting method cannot put any bound in the region $-0.25 < a_* < 1.25$ and $-5 < \epsilon_3 < 15$ if the object does not rotate very fast).

ACKNOWLEDGMENTS

I wish to thank Matteo Guainazzi, for useful comments and suggestions, and Zilong Li, for help in the preparation of the manuscript. This work was supported by the Thousand Young Talents Program, Fudan University, and the Humboldt Foundation.

-
- [1] J. Kormendy and D. Richstone, *Ann. Rev. Astron. Astrophys.* **33**, 581 (1995); R. A. Remillard and J. E. McClintock, *Ann. Rev. Astron. Astrophys.* **44**, 49 (2006) [astro-ph/0606352].
- [2] B. Carter, *Phys. Rev. Lett.* **26**, 331 (1971); D. C. Robinson, *Phys. Rev. Lett.* **34**, 905 (1975); P. T. Chrusciel, J. L. Costa and M. Heusler, *Living Rev. Rel.* **15**, 7 (2012) [arXiv:1205.6112 [gr-qc]].
- [3] R. Penrose, *Riv. Nuovo Cim. Numero Speciale* **1**, 252 (1969) [*Gen. Rel. Grav.* **34**, 1141 (2002)].
- [4] S. N. Zhang, W. Cui and W. Chen, *Astrophys. J.* **482**, L155 (1997) [astro-ph/9704072]; L. -X. Li, E. R. Zimmerman, R. Narayan and J. E. McClintock, *Astrophys. J. Suppl.* **157**, 335 (2005) [astro-ph/0411583]; J. E. McClintock, R. Narayan, S. W. Davis, L. Gou, A. Kulkarni, J. A. Orosz, R. F. Penna and R. A. Remillard *et al.*, *Class. Quant. Grav.* **28**, 114009 (2011) [arXiv:1101.0811 [astro-ph.HE]].
- [5] A. C. Fabian, K. Iwasawa, C. S. Reynolds and A. J. Young, *Publ. Astron. Soc. Pac.* **112**, 1145 (2000) [astro-ph/0004366]; C. S. Reynolds and M. A. Nowak, *Phys. Rept.* **377**, 389 (2003) [astro-ph/0212065].
- [6] F. D. Ryan, *Phys. Rev. D* **52**, 5707 (1995).
- [7] K. Glampedakis and S. Babak, *Class. Quant. Grav.* **23**, 4167 (2006) [arXiv:gr-qc/0510057]; L. Barack and C. Cutler, *Phys. Rev. D* **75**, 042003 (2007) [arXiv:gr-qc/0612029].
- [8] N. Wex and S. Kopeikin, *Astrophys. J.* **514**, 388 (1999) [astro-ph/9811052].
- [9] C. M. Will, *Astrophys. J.* **674**, L25 (2008) [arXiv:0711.1677 [astro-ph]].
- [10] C. Bambi and E. Barausse, *Astrophys. J.* **731**, 121 (2011) [arXiv:1012.2007 [gr-qc]].
- [11] C. Bambi, *Astrophys. J.* **761**, 174 (2012) [arXiv:1210.5679 [gr-qc]].
- [12] C. Bambi, *Phys. Rev. D* **85**, 043002 (2012) [arXiv:1201.1638 [gr-qc]]; *Phys. Rev. D* **86**, 123013 (2012) [arXiv:1204.6395 [gr-qc]].
- [13] C. Bambi, *Phys. Rev. D* **83**, 103003 (2011) [arXiv:1102.0616 [gr-qc]]; *Mod. Phys. Lett. A* **26**, 2453 (2011) [arXiv:1109.4256 [gr-qc]]; *Phys. Lett. B* **705**, 5 (2011) [arXiv:1110.0687 [gr-qc]]; *Phys. Rev. D* **85**, 043001 (2012) [arXiv:1112.4663 [gr-qc]]; arXiv:1205.4640 [gr-qc]; *JCAP* **1209**, 014 (2012) [arXiv:1205.6348 [gr-qc]]; arXiv:1301.0361 [gr-qc].
- [14] C. Bambi, *Europhys. Lett.* **94**, 50002 (2011) [arXiv:1101.1364 [gr-qc]]; *JCAP* **1105**, 009 (2011) [arXiv:1103.5135 [gr-qc]]; Z. Li and C. Bambi, arXiv:1212.5848 [gr-qc].
- [15] C. Bambi and E. Barausse, *Phys. Rev. D* **84**, 084034 (2011) [arXiv:1108.4740 [gr-qc]].
- [16] T. Johannsen and D. Psaltis, arXiv:1202.6069 [astro-ph.HE].
- [17] T. Johannsen and D. Psaltis, *Astrophys. J.* **716**, 187 (2010) [arXiv:1003.3415 [astro-ph.HE]]; *Adv. Space Res.* **47**, 528 (2011) [arXiv:1008.3902 [astro-ph.HE]]; *Astrophys. J.* **726**, 11 (2011) [arXiv:1010.1000 [astro-ph.HE]].
- [18] S. Chen and J. Jing, *Phys. Rev. D* **85**, 124029 (2012) [arXiv:1204.2468 [gr-qc]]; *Phys. Lett. B* **711**, 81 (2012) [arXiv:1110.3462 [gr-qc]].
- [19] C. Liu, S. Chen and J. Jing, *Astrophys. J.* **751**, 148 (2012) [arXiv:1207.0993 [gr-qc]]; *JHEP* **1208**, 097 (2012) [arXiv:1208.1072 [gr-qc]].
- [20] H. Krawczynski, *Astrophys. J.* **754**, 133 (2012)

- [arXiv:1205.7063 [gr-qc]].
- [21] R. A. Konoplya and A. Zhidenko, arXiv:1210.8430 [gr-qc].
- [22] C. Bambi and K. Freese, Phys. Rev. D **79**, 043002 (2009) [arXiv:0812.1328 [astro-ph]]; C. Bambi, K. Freese and R. Takahashi, in *Windows on the Universe*, edited by L. Celnikier et al. (The Gioi Publishers, Ha Noi, Vietnam, 2010), pp. 575-578 [arXiv:0908.3238 [astro-ph.HE]]; C. Bambi and N. Yoshida, Class. Quant. Grav. **27**, 205006 (2010) [arXiv:1004.3149 [gr-qc]]; T. Johannsen and D. Psaltis, Astrophys. J. **718**, 446 (2010) [arXiv:1005.1931 [astro-ph.HE]]; C. Bambi, F. Caravelli and L. Modesto, Phys. Lett. B **711**, 10 (2012) [arXiv:1110.2768 [gr-qc]].
- [23] T. Johannsen and D. Psaltis, Phys. Rev. D **83**, 124015 (2011) [arXiv:1105.3191 [gr-qc]].
- [24] A. C. Fabian, M. J. Rees, L. Stella and N. E. White, Mon. Not. Roy. Astron. Soc. **238**, 729 (1989).
- [25] Y. Tanaka, K. Nandra, A. C. Fabian, H. Inoue, C. Otani, T. Dotani, K. Hayashida and K. Iwasawa *et al.*, Nature **375**, 659 (1995).
- [26] T. J. Turner, L. Miller, J. N. Reeves and S. B. Kraemer, Astron. Astrophys. **475**, 121 (2007); L. Titarchuk, P. Laurent and N. Shaposhnikov, Astrophys. J. **700**, 1831 (2009) [arXiv:0906.1490 [astro-ph.HE]]; L. Miller, T. J. Turner and J. N. Reeves, Mon. Not. Roy. Astron. Soc. **399**, L69 (2009).
- [27] A. Martocchia, V. Karas and G. Matt, Mon. Not. Roy. Astron. Soc. **312**, 817 (2000) [astro-ph/9910562].